Environmental Science & Technology

pubs.acs.org/est

Article

Chlorinated Byproduct Formation during the Electrochemical Advanced Oxidation Process at Magnéli Phase Ti_4O_7 Electrodes

Meng-Hsuan Lin, Devon Manley Bulman, Christina K. Remucal, and Brian P. Chaplin*

Cite This: *Environ. Sci. Technol.* 2020, 54, 12673−12683

Read Online

ACCESS | Metrics & More | Article Recommendations | Supporting Information

ABSTRACT: This research investigated chlorinated byproduct formation at Ti_4O_7 anodes. Resorcinol was used as a model organic compound representative of reactive phenolic groups in natural organic matter and industrial phenolic contaminants and was oxidized in the presence of NaCl (0—5 mM). Resorcinol mineralization was >68% in the presence and absence of NaCl at 3.1 V/SHE (residence time = 13 s). Results indicated that ∼4.3% of the initial chloride was converted to inorganic byproducts (free Cl_2, ClO_2^-, ClO_3^-) in the absence of resorcinol, and this value decreased to <0.8% in the presence of resorcinol. Perchlorate formation rates from chlorate oxidation were 115—371 mol m^{-2} h^{-1}, approximately two orders of magnitude lower than reported values for boron-doped diamond anodes. Liquid chromatography−mass spectroscopy detected two chlorinated organic products. Multichlorinated alcohol compounds ($C_3H_2Cl_4O$ and $C_3H_4Cl_4O$) at 2.5 V/SHE and a monochlorinated phenolic compound ($C_8H_7O_4Cl$) at 3.1 V/SHE were proposed as possible structures. Density functional theory calculations estimated that the proposed alcohol products were resistant to direct oxidation at 2.5 V/SHE, and the $C_8H_7O_4Cl$ compound was likely a transient intermediate. Chlorinated byproducts should be carefully monitored during electrochemical advanced oxidation processes, and multibarrier treatment approaches are likely necessary to prevent halogenated byproducts in the treated water.

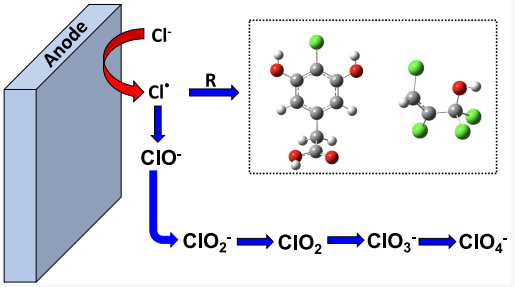

INTRODUCTION

Electrochemical advanced oxidation processes (EAOPs) have been researched as possible new modular technologies for drinking water treatment,[1] industrial wastewater treatment,[2−4] and groundwater remediation.[5,6] EAOPs rely on stable anode materials that primarily degrade contaminants through direct oxidation reactions at the anode surface and indirect oxidation through reactions with hydroxyl radicals ($OH^•$) that form from the oxidation of water.[7,8] Boron-doped diamond (BDD) electrodes are currently considered to be the state-of-the-art anode for EAOPs because they generate high yields of $OH^•$ and are anodically stable, corrosion resistant, and commercially available.[9,10] However, the application of BDD electrodes for treatment of chloride-containing waters results in the formation of inorganic and organic chlorinated byproducts,[7,8,11−18] which have documented health risks such as bladder cancer and birth defects.[19,20]

The generation of inorganic chlorinated byproducts during EAOPs is initiated by the oxidation of chloride (Cl^-) at the anode surface. The general oxidation pathway is shown:

$$Cl^- \rightarrow Cl^• \rightarrow HOCl/OCl^- \rightarrow ClO_2^- \rightarrow ClO_2 \rightarrow ClO_3^- \rightarrow ClO_4^- \quad (1)$$

where chlorine is oxidized from an initial oxidation state of −1 in Cl^- to +7 in perchlorate (ClO_4^-). The electrochemical formation of chlorite (ClO_2^-), chlorate (ClO_3^-), and ClO_4^- has been reported in studies using BDD electrodes.[7,16−18] The U.S. Environmental Protection Agency (EPA) has set a maximum contaminant level (MCL) for ClO_2^- in drinking water at 1.0 mg L^{-1} and proposed a nonenforceable MCL goal (MCLG) for ClO_4^- at 56 μg L^{-1}.[21] In addition, Massachusetts and California have set more stringent, enforceable drinking water standards for ClO_4^- of 2 μg L^{-1} and 6 μg L^{-1}, respectively.[22,23] Currently, ClO_3^- is not regulated, but the EPA has set a health reference level (HRL) at 210 μg L^{-1}.[24]

Organic chlorinated byproducts may also form during EAOPs through reactions between organic compounds and chlorine species shown in reaction 1, such as chlorine radical ($Cl^•$), hypochlorous acid/hypochlorite ($HOCl/OCl^-$), and chlorine dioxide (ClO_2). For example, the electrochemical treatment of saline waters using BDD anodes formed trihalomethanes (THMs), haloacetic acids (HAAs), haloacetonitriles, haloketones, 1,2-dichloroethane, and unidentified adsorbable organic chlorine compounds.[11−15] The EPA has set MCLs in drinking water for THMs and HAAs at a combined

Received: June 16, 2020
Revised: August 21, 2020
Accepted: August 25, 2020
Published: August 25, 2020

https://dx.doi.org/10.1021/acs.est.0c03916
Environ. Sci. Technol. 2020, 54, 12673−12683

concentration of 80 μg L^{-1} for four regulated THMs and 60 μg L^{-1} for five regulated HAAs.[25] Several other halogenated industrial organic chemicals have also been regulated by the EPA at the μg L^{-1} range. Because of the health concerns associated with both regulated and unregulated halogenated organic compounds, close scrutiny of unintended byproducts that form during EAOPs is necessary so that appropriate treatment trains can be developed for a given water treatment application.

Recent work has shown that porous Magnéli phase Ti_4O_7 electrodes are high surface area, stable anode materials[26,27] that are capable of direct oxidation of contaminants[28] and formation of $OH^{\bullet}$.[27] When operated in flow-through mode, Ti_4O_7 anodes achieve over an order of magnitude higher mass transport rates compared to traditional parallel plate electrochemical cells (e.g., BDD).[29] The combination of enhanced mass transport and high specific surface area results in significant removal of various organic contaminants with high rate constants and low energy consumption, even when operated in a single-pass mode with short hydraulic residence times (~10 s).[28−34] However, work has not yet been done to determine the potential for halogenated byproduct formation during their use in EAOPs.

Therefore, the aim of this study was to investigate both inorganic and organic chlorinated byproduct formation during EAOPs using a Magnéli phase Ti_4O_7 reactive electrochemical membrane (REM). Since phenolic compounds play a central role in the structure of natural organic matter (NOM) and many industrial contaminants present in natural waters,[35−37] resorcinol was used as a model organic compound, and it was oxidized in the presence of NaCl (1 and 5 mM) and as a function of electrode potential. Inorganic and organic byproduct formation was characterized using ion chromatography and liquid chromatography−mass spectrometry (LC−MS), respectively. The stability and probable fate of resorcinol and chlorinated byproducts were investigated using density functional theory (DFT) methods. This work is the critical first step in understanding halogenated byproduct formation on Ti_4O_7 electrodes.

MATERIALS AND METHODS

Reagents. Sodium chloride (NaCl), sodium chlorite ($NaClO_2$), sodium chlorate ($NaClO_3$), potassium phosphate monobasic (KH_2PO_4), and HPLC grade methanol were purchased from Alfa Aesar (MA, USA). Sodium perchlorate ($NaClO_4$), sodium hypochlorite solution (NaOCl, 10−15 wt/vol % available chlorine), and titanium dioxide (TiO_2) were purchased from Sigma-Aldrich (MO, USA). Resorcinol was purchased from MP Biomedical (OH, USA). Paraffin oil was purchased form EMD Millipore (USA). Sodium sulfite (Na_2SO_3) was purchased from Thermo Fisher (MA, USA). Chemical Oxygen Demand (COD) reagents were purchased from Hach (CO, USA). Solutions were made with deionized (DI) water (18.2 MΩ cm at 21 °C). All chemicals were used as received.

REM Synthesis and Characterization. REMs were synthesized using a previously published method.[38] Briefly, 5 g of TiO_2 powder (particle diameter = 32 nm) was reduced to Ti_4O_7 in a tube furnace at 1050 °C for 6 h in the presence of 1 atm H_2 gas (flow rate = 252 cm^3 min^{-1}). The Ti_4O_7 powder (0.65 g) was mixed with 1.25 wt % paraffin oil as a binder. The mixture was compressed in a 1.12 cm diameter die with a uniaxial pressure of 2.7 MPa. The thickness of the pellet was approximately 2 mm. Pellets were placed in a tube furnace at 1050 °C for 6 h in the presence of 1 atm H_2 for sintering. The Magnéli phases present in the pellet were determined by XRD (Siemens D-5000) with Cu−K-radiation (λ = 1.5418 Å), and diffraction peaks were identified according to the standard database.[39,40]

Experimental Flow-through Reactor Setup. A schematic of the reactor setup is shown in the Supporting Information (SI) (Figure S1). Experiments were performed in a flow-through reactor in single-pass mode with a standard three-electrode setup (Figure S1a). The Ti_4O_7 REM was used as the working electrode (anode) with an exposed projected surface area of 0.5 cm^2. The current collector was Ti, and a 0.35 cm^2 BDD film on Nb (BDD/Nb) ring electrode was placed between the Ti and REM to prevent Ti corrosion in the presence of reactive chlorine species (Figure S1b). The BDD/Nb electrode did not participate significantly in the reactions, as shown in the SI (Figure S2). The interelectrode gap was 2 mm, and the counter electrode (cathode) was Ti. A 1 mm diameter leak-free Ag/AgCl was used as the reference electrode (Warner Instruments, LF-100, CT, USA) (Figure S1b). Permeate flux (J = 240 L m^{-2} h^{-1} (LMH)) was controlled and adjusted using a digital gear micropump (Cole-Parmer, IL, USA). Applied potentials and currents were controlled and measured by a Gamry Reference 600 potentiostat/galvanostat (PA, USA). All potentials were corrected for potential drop in solution (iR_s) and reported versus the standard hydrogen electrode (/SHE).

Electrochemical Oxidation Experiments. All oxidation experiments were conducted in the flow-through reactor at 22 ± 1 °C, pH = 6.7, and a solution conductivity of 283 μS cm^{-1} using a 6 to 10 mM KH_2PO_4 background electrolyte and 0 to 5 mM NaCl addition. The KH_2PO_4 electrolyte was used because it is relatively inert to electrochemical oxidation. The solution conductivity value was chosen to mimic that of typical natural waters[41] and was measured using a conductivity probe (PC2700, Oakton, Cole-Parmer, IL, USA). Control oxidation experiments were performed with either 1 mM resorcinol or NaCl (1 and 5 mM) to determine a baseline for resorcinol oxidation and inorganic chlorinated byproduct formation. The following potentials were applied during electrochemical oxidation experiments: open circuit potential (OCP = 0.11 V/SHE), 0.99 ± 0.09, 1.56 ± 0.03, 2.07 ± 0.04, 2.50 ± 0.04, and 3.10 ± 0.03 V/SHE. Two solution conditions were used to study chlorinated byproduct formation: (1) 1 mM NaCl and 1 mM resorcinol; and (2) 5 mM NaCl and 1 mM resorcinol. All experiments were performed in duplicate, and errors reported represent 95% confidence intervals on average values. The 1 mM concentration of resorcinol, although high for NOM, was chosen to ensure transformation product detection, and the 1—5 mM NaCl concentrations were chosen to bracket the Cl^- concentrations found in typical natural waters.[42]

Separate experiments were conducted to measure the kinetics of ClO_4^- formation from a 1 mM $NaClO_3$/10 mM KH_2PO_4 solution under OCP and 3.0 V/SHE with flow rates of 240 to 1200 LMH. To compare with the electrochemical system, batch control experiments were also conducted in a beaker containing 1 mM NaOCl, 1 mM resorcinol, and KH_2PO_4 electrolyte under constant mixing.

Analytical Methods. The permeate samples were split during collection. One part was immediately quenched with Na_2SO_3 and used for further analyses; the other part was used for free chlorine measurements. Concentrations of Cl^-, ClO_2^-,

https://dx.doi.org/10.1021/acs.est.0c03916
Environ. Sci. Technol. 2020, 54, 12673−12683

ClO_3^-, and ClO_4^- were determined by ion chromatography (Dionex ICS-2100; Dionex Ion Pac AS16 column; KOH eluent; 0.75 mL min^{-1} flow rate) with method detection limits of 10 nM for ClO_2^-, ClO_3^-, and ClO_4^- and 5 nM for Cl^-. Free chlorine (as Cl_2) concentrations were determined by Hach method 8021[43] according to the manufacturer's protocol and consisted of HOCl and OCl^- under the pH conditions of the experiments. The Cl^- concentration was calculated by subtracting the measured free chlorine concentration from the IC measured Cl^- concentration, where the latter was quenched with Na_2SO_3. The total moles of Cl were calculated using eq 2:

$$\text{Total moles of Cl} = 2 \times \text{Free Chlorine } (Cl_2) + Cl^- + ClO_2^- + ClO_3^- + ClO_4^- \quad (2)$$

Resorcinol concentrations were determined using a Shimadzu UFLC XR HPLC with a Phenomenex Kinetex 5 μm C18 column (5 μm, 100 Å, 250 × 4.6 mm^2) and a photodiode array detector (PDA) (Nexera X2, Shimadzu). The mobile phase was 75:25 (%, v/v) mixture of methanol and DI water with a flow rate of 1.0 mL min^{-1}. The PDA detector was set to 254 nm for resorcinol analysis.[43−45] COD measurements were used to estimate resorcinol mineralization according to the manufacturer's protocol.[46]

Select samples were analyzed by negative mode electrospray ionization liquid chromatography−mass spectrometry (LC−MS; Agilent 1260 HPLC coupled to an Agilent 6460 triple-quad MS). Elutions were achieved using an Agilent Poroshell 120 EC-C18 column with 0.1% formic acid (10% acetonitrile, v/v) and acetonitrile as the aqueous and mobile phases, respectively, at a flow rate of 0.25 mL/min. The mass-to-charge ratios (m/z) of chlorinated compounds were identified from a full MS scan from 25−500 m/z based on the isotopic signature of chlorine. All m/z values measured by LC−MS were converted to Daltons (Da) by adding the mass of one proton after verifying that the ions were singly charged. The differences in the masses of proposed structures and the measured masses may be due to slight differences in the Cl^{35}:Cl^{37} isotope ratios but are within the error of the LC−MS. For all proposed Cl-containing compounds, it was assumed that Cl had a standard molar mass of 35.45 Da.

Quantum Mechanical Simulations. DFT simulations were performed using Gaussian 16 software.[47] Unrestricted spin, all-electron calculations were performed using the 6-31G ++(d) basis set for frequency, geometry optimization, and energy calculations. The M06-2X hybrid meta exchange-correlation functionals were used,[48] and implicit water solvation was simulated using the SMD model.[49] Individual explicit water molecules were incorporated into simulations where appropriate to simulate important hydrogen bonding interactions.

Direct electron transfer reactions were modeled using Marcus theory, according to methods described previously.[33,50] The E^0 values for a given direct electron transfer reaction were calculated by the following equation:

$$E^0 = -\frac{\Delta_r G^\circ}{nF} - E_{abs}{}^0(SHE) \quad (3)$$

where $\Delta_r G^0$ is the standard free energy for the reduction reaction, F is the Faraday constant, n is the number of electrons transferred, and $E_{abs}{}^0$ (SHE) is the absolute standard reduction potential of the SHE ($E_{abs}{}^0$ (SHE) = 4.28 eV).[51,52]

The potential dependent Gibbs free energy of activation ($\Delta G^\ddagger$) for direct electron transfer oxidation reactions were calculated using Marcus theory according to the following equation:[53]

$$\Delta G^\ddagger = \frac{\lambda_f}{4}\left[1 - \frac{96.5(E - E^0)}{\lambda_f}\right]^2 \quad (4)$$

where E is the applied electrode potential, and λ_f is the total reorganization energy of the forward oxidation reaction. The effect of the solvent on λ_f was not considered as previous research showed negligible solvent effects in polar solvents.[54]

RESULTS AND DISCUSSION

Resorcinol Oxidation Experiments. The Ti_4O_7 Magnéli phase reactive electrochemical membranes (REMs) used in this study were thoroughly characterized in prior work.[38] The conductivity of the REM was 765 S m^{-1}, and the XRD pattern contained the characteristic peak at 20.8° and other peaks that matched the Ti_4O_7 standard data (Figure 1a). A schematic showing the possible electrochemical reaction pathways for resorcinol and chloride oxidation is shown in Figure S3. Control oxidation experiments were conducted containing only 1 mM resorcinol (flux = 240 LMH; KH_2PO_4 electrolyte; solution conductivity = 283 μS cm^{-1}; pH = 6.7). Under OCP conditions (0.11 V/SHE), resorcinol removal was not observed (Figure 1b), which indicated that it did not significantly adsorb on the REM. Measurable resorcinol oxidation began at potentials >1.0 V/SHE, and average normalized permeate resorcinol concentrations (C_p/C_f) for duplicate experiments were 0.80 ± 0.01, 0.52 ± 0.001, 0.29 ± 0.01, and 0.12 ± 0.01 at anodic potentials of 1.6, 2.1, 2.5, and 3.1 V/SHE, respectively. The OCP, 2.5, and 3.1 V/SHE were used for subsequent resorcinol electrochemical oxidation experiments, which is a realistic potential range for which electrochemical oxidation would be used in a treatment scenario. The current densities for each set of experiments are provided in Table S1.

To investigate chlorinated byproduct formation, NaCl concentrations of 1 and 5 mM were added to 1 mM resorcinol. Resorcinol permeate concentration profiles indicated that the addition of NaCl to solution had a small but observable effect on resorcinol removal (Figure S4). For example, the average resorcinol C_p/C_f values for duplicate 1 mM resorcinol experiments without NaCl were 0.29 ± 0.01 and 0.12 ± 0.01 at 2.5 and 3.1 V/SHE, respectively. These values increased to 0.38 ± 0.02 and 0.20 ± 0.01 for the 1 mM resorcinol/1 mM NaCl solutions and were 0.35 ± 0.03 and 0.14 ± 0.02 for the 1 mM resorcinol/5 mM NaCl solutions at applied potentials of 2.5 and 3.1 V/SHE, respectively. In addition, the C_p/C_f values for COD were used to estimate the extent of resorcinol mineralization (Figure S4). Estimates of mineralization at 2.5 V/SHE were 60 ± 0.3%, 68 ± 6%, and 57 ± 9%, and estimates at 3.1 V/SHE were 74 ± 1%, 69 ± 6%, and 68 ± 3% at 0, 1, and 5 mM NaCl concentrations, respectively. Results show an increase in resorcinol mineralization as a function of potential but do not show a trend with respect to NaCl concentration. Resorcinol mineralization was >60% in a single pass through the REM in all experiments, and the overall oxidation half-reaction is shown in reaction 5:

$$C_6H_6O_2 + 10H_2O \rightarrow 6CO_2 + 26H^+ + 26e^- \quad (5)$$

https://dx.doi.org/10.1021/acs.est.0c03916
Environ. Sci. Technol. 2020, 54, 12673−12683

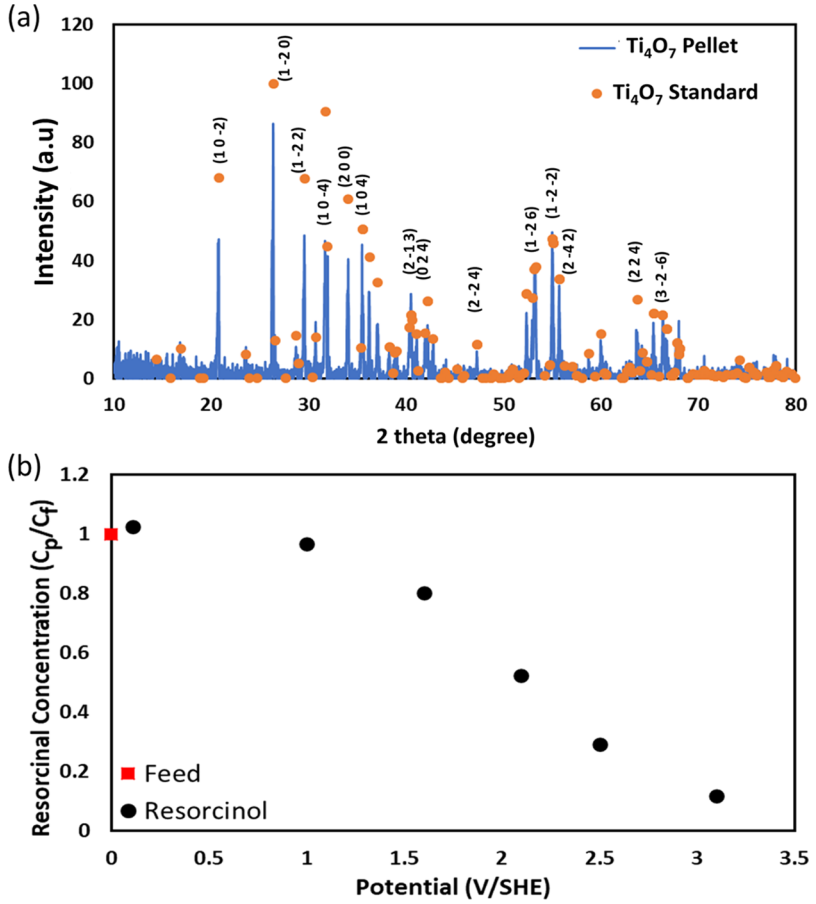

Figure 1. (a) XRD analysis of Ti_4O_7 pellet (blue line) and the standard diffraction data of Ti_4O_7 (JCPDS. No. 50−0787) (orange dots). (b) Normalized resorcinol concentration profiles (C_p/C_f) in the feed (red square) and permeate (black dots) without NaCl addition. Experiments had a flux of 240 LMH and retention time of 13 s. Error bars are contained within the data points.

Electrochemical Byproduct Formation. The formation of inorganic chlorinated byproducts was investigated in two sets of experiments: (1) NaCl-only controls with 1 and 5 mM NaCl and (2) 1 mM resorcinol containing either 1 or 5 mM NaCl. Results from oxidation of a 1 mM NaCl solution are shown in Figure 2a and are reported as a percentage of the feed Cl^- concentration at log-scale. Only 6.0 ± 4.0% to 7.0 ± 2.0% of Cl^- was oxidized at anodic potentials between 1.0 to 3.1 V/SHE, indicating slow reaction kinetics for Cl^- at the Ti_4O_7 surface compared to resorcinol oxidation. Inorganic chlorinated compounds were limited to free Cl_2 (i.e., HOCl + OCl^-) at concentrations between 5.1 and 21 μM (1.0 to 4.3% of feed Cl^-), and approximately 0.7 μM of ClO_2^- (0.070% of feed Cl^-) was detected at an anodic potential of 3.1 V/SHE (Figure 2a). Neither ClO_3^- nor ClO_4^- was detected (<10 nM) during the oxidation of the 1 mM NaCl solution. The oxidation products from a 5 mM NaCl solution are shown in Figure 2c. Chloride oxidation was between 3.0 ± 4.0% at 1.0 V/SHE and 6.0 ± 2.0% at 3.1 V/SHE. Oxidized inorganic chlorinated species included free Cl_2 (6.5 to 110 μM; 0.26 to 4.4% of feed Cl^-), ClO_2^- (0.1 to 2.5 μM; 0.0020 to 0.050% of feed Cl^-), ClO_3^- (6.0 to 8.0 μM; 0.12 to 0.16% of feed Cl^-), and low concentrations of ClO_4^- of 0.3 μM (30 μg L^{-1}; 0.0060% of feed Cl^-) at 1.6 V/SHE and 3.1 V/SHE (Figure 2c). Perchlorate was not detected at 2.1 and 2.5 V/SHE, which may be due to the evolution of different functional groups on the Ti_4O_7 electrode as a function of potential. Prior work has shown that ClO_4^- formation is highly sensitive to functional groups at BDD electrodes.[17,18] However, more research is needed to test this hypothesis for Ti_4O_7 electrodes. The ClO_4^- concentrations were lower than the EPA's proposed MCLG for perchlorate (56 μg L^{-1}), and ClO_3^- concentrations were close to the EPA's HRL. The highest measured conversion of Cl^- to inorganic byproducts in the 1 mM NaCl solution was 4.3% at 2.5 V/SHE and in the 5 mM NaCl solution was 4.5% at 2.5 V/SHE. The total measured inorganic chlorinated byproducts were not significantly different from the total Cl^- conversion.

The inorganic chlorinated byproducts that formed during the oxidation of resorcinol in NaCl solutions were similar to the NaCl-only control experiments, and Cl^- oxidation was 10 ± 1% at both anodic potentials of 2.5 and 3.1 V/SHE. Permeate solutions contained low concentrations of free Cl_2 (1.1 and 4.0 μM; 0.22 and 0.80% of feed Cl^-) in the 1 mM NaCl/resorcinol solution (Figure 2b) and free Cl_2 (5.0 and 7.0 μM; 0.20 and 0.28% of feed Cl^-), ClO_2^- (2.0 μM; 0.040% of feed Cl^-), and ClO_3^- (3.5 and 3.0 μM; 0.070 and 0.060% of feed Cl^-) in the 5 mM NaCl/1 mM resorcinol solution (Figure 2d). Perchlorate was detected at a low concentration (0.3 μM; 0.0060% of feed Cl^-) in the 5 mM NaCl control but was not detected in the 5 mM NaCl/1 mM resorcinol experiments, similar to prior work that concluded that ClO_4^- formation is lower in chloride solutions that contain organic compounds.[55] In fact, all inorganic chlorinated products were lower in the presence of resorcinol (comparing Figure 2a and b to Figure 2c and d) due to the competition for reactive sites and available oxidants and reactions between organics and

https://dx.doi.org/10.1021/acs.est.0c03916
Environ. Sci. Technol. 2020, 54, 12673−12683

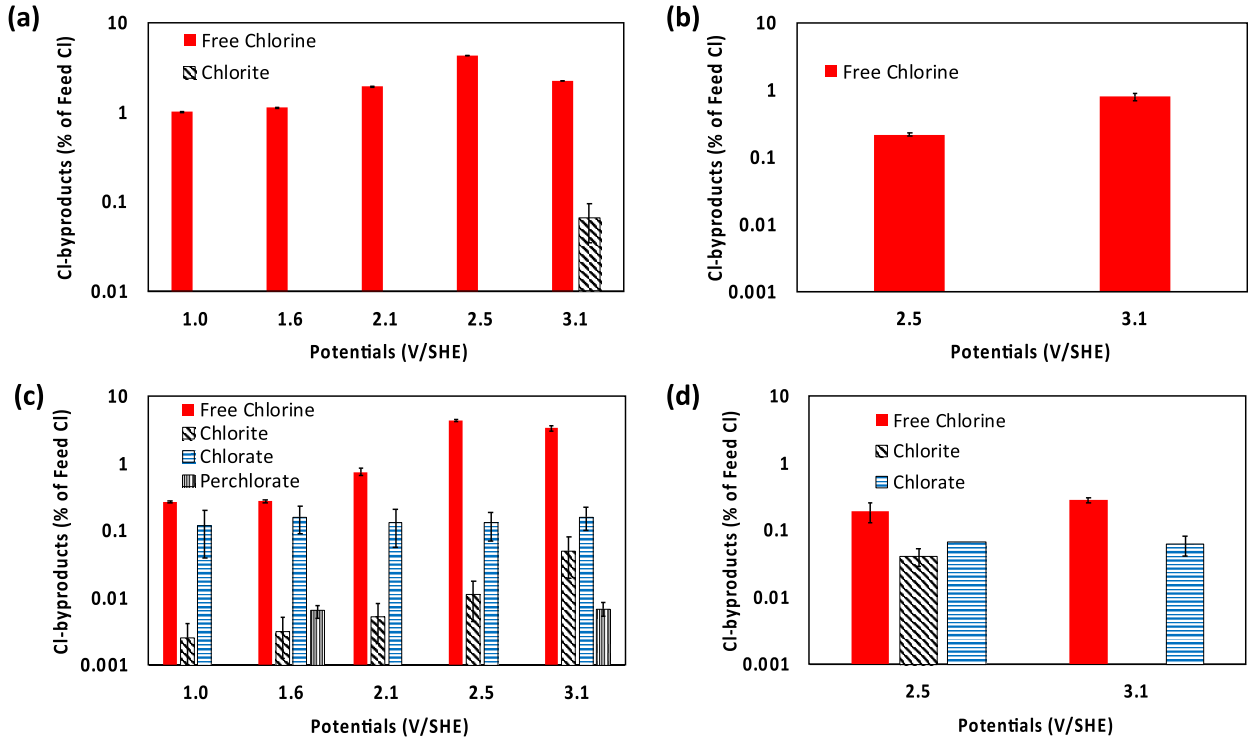

Figure 2. Inorganic chlorinated byproducts detected during oxidation experiments: (a) 1 mM NaCl; (b) 1 mM NaCl and 1 mM resorcinol; (c) 5 mM NaCl; and (d) 5 mM NaCl and 1 mM resorcinol. All experiments had KH_2PO_4 background electrolyte, solution conductivity = 283 μS/cm, solution pH = 6.7, and J = 240 LMH.

chlorinated inorganic oxidants. The highest measured conversion of Cl^- to inorganic byproducts in the 1 mM NaCl/1 mM resorcinol solution was 0.8% at 3.1 V/SHE and in the 5 mM NaCl/1 mM resorcinol solution was 0.3% at 2.5 V/SHE. The total measured inorganic chlorinated byproducts were much lower than the total Cl^- conversion, indicating that chlorinated organic byproducts formed.

Since ClO_4^- is a terminal oxidation product of Cl^-, it has potential to accumulate in solution under conditions of extended electrolysis (e.g., batch mode oxidation). Therefore, separate experiments were conducted to investigate ClO_4^- formation with a 1 mM $NaClO_3$ feed solution at an anodic potential of 3.0 V/SHE and as a function of flow rate (Figure S5). Results from these experiments yielded a first order rate constant of 0.04 s^{-1} for ClO_4^- formation, and permeate ClO_4^- concentrations ranged between 31 to 48 $\mu g\ L^{-1}$, for hydraulic residence times between 2.6 to 13 s, respectively (Figure S5a). These concentrations yield projected surface area normalized rates between 115 and 371 $\mu mol\ m^{-2}\ h^{-1}$ (Figure S5b), which are approximately three orders of magnitude lower if normalized by the total REM surface area (0.07 and 0.21 $\mu mol\ m^{-2}\ h^{-1}$; total surface area = 883 cm^2).[38] Furthermore, the ClO_4^- concentrations in our experiments were always lower than the EPA's MCLG of 56 $\mu g\ L^{-1}$.[21] These experiments represent the worst-case scenario for ClO_4^- formation, as they were conducted with high ClO_3^- concentration (1 mM) and in the absence of organic compounds. A previous study with a rotating disk electrode (RDE) setup and under similar reaction conditions (i.e, 1 mM $NaClO_3$, anode potential of 2.6 to 2.7 V/SHE, pH 4.5) measured ClO_4^- formation rates from ClO_3^- on BDD electrodes between 28 000 and 45 000 $\mu mol\ m^{-2}\ h^{-1}$,[17] which are over two orders of magnitude higher than our projected surface area normalized rates and five orders of magnitude higher than our total surface area normalized rates. The mass transfer rate constant for the RDE setup in the BDD study was estimated at 3.7×10^{-4} m s^{-1} using the Levich equation,[17] which is comparable to previous values reported in our REM flow-through reactor ($3.0–4.5 \times 10^{-4}$ m s^{-1}).[38] Since the mechanism of ClO_4^- formation from ClO_3^- is not pH dependent,[17] comparison of our results to the BDD study is appropriate. These results show the low production rate of ClO_4^- on the Ti_4O_7 REM anodes compared to BDD.

During the oxidation of resorcinol to CO_2, it was assumed that various radicals formed and reacted with each other to form a diverse set of products. To characterize the primary stable products during this process, permeate solutions from resorcinol oxidation were analyzed by LC–MS (Figure 3). The raw LC–MS data are provided in the Supporting Information, and isotopic patterns were used to identify chlorinated products (Figures S6 and S7). Resorcinol oxidation in NaCl-free solutions at potentials of 2.5 and 3.1 V/SHE resulted in nonchlorinated products with observed masses of 110.1, 116, 154.1, 187.2, and 218 Da (Figure 3). The 110.1 Da product had the same mass as resorcinol but a different retention time, indicating it was an oxidation product. Under OCP conditions, products were not observed, which was in agreement with the lack of resorcinol transformation (Figure 1b). Products were not detected with a mass less than resorcinol (110.1 Da), indicating that higher molecular weight compounds formed from the coupling of radical carbon species and addition of $OH^•$ during the reaction. Resorcinol oxidation in the presence of 1.0 and 5.0 mM NaCl caused a slight decrease in the peak areas of the nonchlorinated oxidation products relative to the NaCl-free experiments at both 2.5 and 3.1 V/SHE (Figure 3),

https://dx.doi.org/10.1021/acs.est.0c03916
Environ. Sci. Technol. 2020, 54, 12673–12683

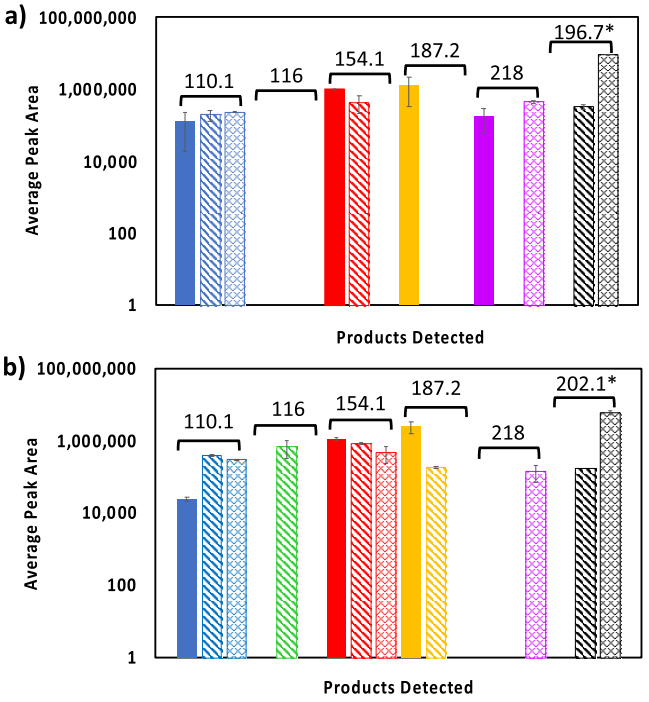

Figure 3. Organic and chlorinated byproducts formation in the permeate solution during oxidation process with applied potential (a) 2.5 V/SHE and (b) 3.1 V/SHE. Mass of organic byproducts were determined by LC−MS (solid = 0 mM NaCl; striped = 1 mM NaCl; hatched = 5 mM NaCl; ∗ = chlorinated product). Table S2 contains a list of the masses of proposed structures.

indicating some competition at the electrode surface between organic species and Cl^- oxidation.

The addition of 1 mM and 5 mM NaCl to solution resulted in the formation of organic chlorinated byproducts (Figure 3). The chlorinated organic byproducts consisted of a chlorinated compound with four Cl atoms and a mass of 196.7 Da at 2.5 V/SHE and a monochlorinated compound with a mass of 202.1 Da at 3.1 V/SHE (Figure 3 and Figure S7). The chlorinated organic byproduct peak areas increased by an order of magnitude by increasing the NaCl concentration from 1 to 5 mM at both 2.5 V/SHE (Figure 3a) and 3.1 V/SHE (Figure 3b). Other chlorinated organic compounds were not detected, suggesting that the chlorinated compounds with masses of 196.7 and 202.1 Da were fairly resistant to further oxidation, oxidized to nonpolar chlorinated organic compounds that were not detected by LC−MS, or mineralized to CO_2, H_2O, and inorganic chlorine species (ClO_x^-, x = 1 to 4).

Free Chlorine Generated Byproducts. Additional control experiments were conducted to determine if the organic chlorinated byproducts that were observed during electrochemical oxidation of resorcinol were a result of reaction with free Cl_2. Therefore, a batch experiment containing equimolar concentrations of 1 mM NaOCl and 1 mM resorcinol in the KH_2PO_4 background electrolyte with the same solution composition as electrochemical experiments was conducted. The 1:1 molar ratio of NaOCl:resorcinol was used to better reflect the anticipated solution conditions near the anode surface, where free Cl_2 concentrations would be higher and resorcinol concentrations lower compared to the bulk solution. The formation of organic chlorinated byproducts was studied using LC−MS analysis, and results are shown in the SI (Figures S8 and S9) for reaction times of 10 and 40 min. The total reaction time between free Cl_2 and resorcinol for electrochemical experiments was approximately 6 min, which corresponded to the time the fluid entered the REM reactor until it was quenched with $NaSO_3$. Organic chlorinated byproducts with masses of 84, 150, and 178 Da were detected in the NaOCl/resorcinol solution (Figures S8 and S9). Structures with masses of 82.5, 150.5, and 178.9 Da were proposed as possible products for the reaction between resorcinol and $HOCl/OCl^-$ (Figure S10 and Table S2) and were based on results from the literature.[55−66] Products include a chlorinated phenolic compound (mass = 178.9 Da) and chlorinated aliphatic compounds (masses = 150.5 and 82.5 Da). The products for direct reaction between resorcinol and $HOCl/OCl^-$ were distinctly different from those for electrochemical oxidation experiments (Figure 3), indicating that oxidation of resorcinol in electrochemical experiments was not solely attributed to reactions with $HOCl/OCl^-$.

Mechanism. DFT modeling was used to interpret the experimental data and to gain insights into probable reaction pathways for the electrochemical oxidation of resorcinol and subsequent chlorinated byproduct formation. The potential dependent $\Delta G^{\ddagger}$ values for the oxidation of resorcinol (R) via direct electron transfer (DET) (reaction 6) were calculated using the Marcus Theory (eq 4):

$$R \rightarrow R^{\bullet +} + e^- \quad (6)$$

The results are shown in Figure 4a, and the optimized $R/R^{\bullet +}$ structures are shown in Figure S11. Modeling determined E° = 1.50 V/SHE and λ_f = 26 kJ mol^{-1}. Figure 4a shows that $\Delta G^{\ddagger}$ = 54 kJ mol^{-1} at 1.0 V/SHE and $\Delta G^{\ddagger}$ = 3.9 kJ mol^{-1} at 1.56 V/SHE. These results are consistent with experimental results where resorcinol degradation began to increase in this potential range (Figure 1b), suggesting the DET was a primary mechanism for resorcinol oxidation at anodic potentials that were too low for $OH^{\bullet}$ formation (i.e., < 2.5 V/SHE).[67] At higher potentials, where $OH^{\bullet}$ formation increases, reaction between $OH^{\bullet}$ and resorcinol will occur with a diffusion-limited rate constant ($k_{OH^{\bullet}, Res.}$ = 1.2 × 10^{10} M^{-1} s^{-1}; pH = 9),[68] indicating that it could also be a contributing mechanism for resorcinol oxidation at anodic potentials >2.5 V/SHE. The combination of $R^{\bullet +}$ and $OH^{\bullet}$ formation and the various radical oxidation and dimerization reactions that are possible can lead to a wide range of products. The masses detected by LC−MS in the NaCl-free solutions (110.1, 116.1, 154.1, 187.2, and 218 Da) can be explained by three general pathways (Scheme 1). Pathway 1, DET reactions that lead to dimerization of $R^{\bullet}$; Pathway 2, $OH^{\bullet}$ attack of R to form ring opening products; and Pathway 3, C fragment addition to R to form substituted phenolic compounds.[7,69,70]

Pathway 1 is proposed to form R dimerization products with a mass of 218 Da. The 218 Da product was detected in the NaCl-free solution at 2.5 V/SHE but not at 3.1 V/SHE (Figure 3), which was attributed to a higher yield of $OH^{\bullet}$ at 3.1 V/SHE that would both break the phenolic ring of R and oxidize any dimerization products that formed. The formation of the 218 Da product was also sensitive to the NaCl concentration. For example, it was not detected in the 1 mM NaCl solutions but was detected at 5 mM NaCl at both potentials (Figure 3). The exact mechanisms responsible for these observations are unclear but are likely a result of reactions between $OH^{\bullet}$ and chlorine species, as well as competition for DET sites at the electrode surface between R, Cl^-, and reaction intermediates.

https://dx.doi.org/10.1021/acs.est.0c03916
Environ. Sci. Technol. 2020, 54, 12673−12683

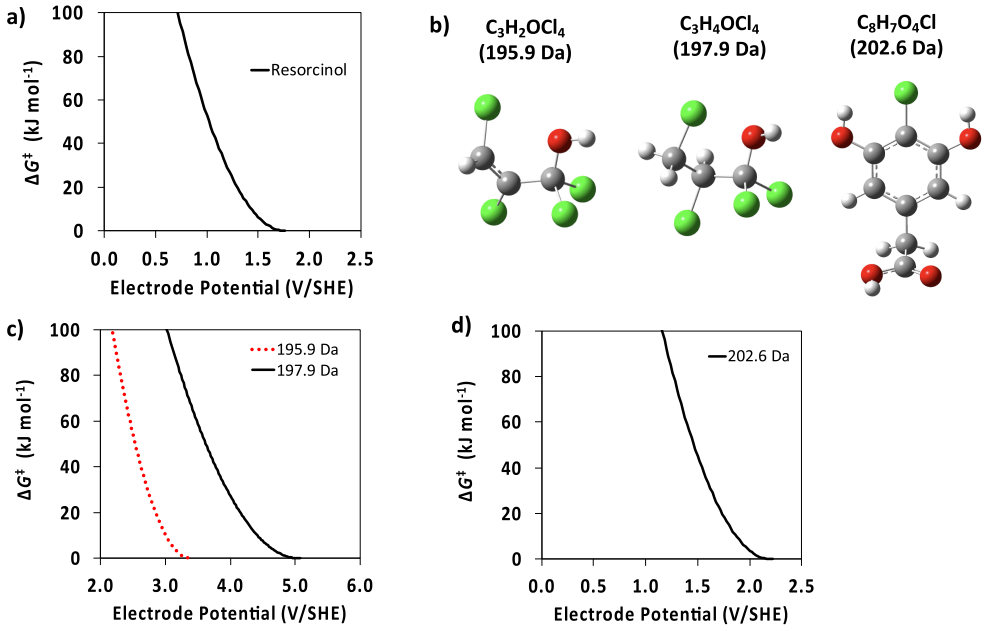

Figure 4. (a) Activation energy for resorcinol. (b) Proposed structures for the 196.7 and 202.1 Da compounds. (c) Activation energy for $C_3H_2OCl_4$ (195.9 Da) and $C_3H_4OCl_4$ (197.9 Da). (d) Activation energy for $C_8H_7O_4Cl$ (202.6 Da). Atom key: carbon = gray; oxygen = red; hydrogen = white; chlorine = green.

Pathway 2 leads to ring opening reactions with proposed C4 products of maleic acid (MA) and fumaric acid (FA), both with mass of 116.1 Da, and the C5 product of cyclopent-4-ene-1,2,3-trione (C), with a mass of 110.1 Da. Both MA and FA have been detected in prior studies of electrochemical oxidation of phenolic compounds.[7,70] The 116 Da product was only detected at 3.1 V/SHE and in the presence of 1 mM NaCl (Figure 3), which indicates that this product was generally a fast reacting intermediate but its rate of degradation was affected by competitive reactions from Cl^-.

Pathway 3 involves the reaction between $R/R^{\bullet+}$ and C fragments that form during the electrochemical oxidation process, forming proposed products of 3,5-dihydroxybenzoic acid (BA), with a mass of 154.1 Da, and 2-(3,5-dihycroxy-cyclohexa-2,4-dien-1-yl)ethane-1,1,2-triol (DHC), with a mass of 188.2 Da. Both of these products were detected with similar peak areas at 2.5 and 3.1 V/SHE, but their detection was highly affected by the NaCl concentration (Figure 3). For example, at 2.5 V/SHE, the 154.1 Da product was not detected at 5 mM NaCl concentration and the 187.2 Da product was not detected at either 1 or 5 mM NaCl concentrations. At 3.1 V/SHE, the 154.1 Da product was detected at both NaCl concentrations, but the 187.2 Da product was not detected at 5 mM NaCl concentration.

The reaction mechanisms responsible for organic chlorinated byproduct formation in the presence of NaCl are more complex and can involve reactions between a wide range of organic compounds, reactive oxygen species, and reactive chlorine species generated during the oxidation process. We propose possible structures for the chlorinated products based on the following constraints: (1) the number of Cl atoms were determined by the isotope data (Figure S7); (2) a close match to the measured m/z value; (3) inclusion of a −OH or −COOH ionizable functional group is needed for the compound to be detected by the LC−MS method; and (4) the compound only contains C, H, O, and Cl.

On the basis of these constraints, we propose two chlorinated alcohol products as candidates for the 196.7 Da product detected during the electrochemical oxidation of R in the presence of NaCl at 2.5 V/SHE. Since the LC−MS data indicated that this compound contained 4 Cl atoms (see Figure S7), possible products of $C_3H_2OCl_4$ and $C_3H_4OCl_4$ were proposed (Figure 4b), which have masses of 195.9 and 197.9 Da, respectively. Previous studies have proposed the formation of C2 and C3 chlorinated ketones and haloacetaldehydes during chlorination and chloramination of phenolic precursors,[64,71] which are similar in structure to our proposed compounds. However, electrochemical oxidation is expected to produce a different suite of chlorinated products, based on the additional DET and $OH^{\bullet}$ oxidation pathways, which could be responsible for the formation of these chlorinated alcohol products. At a potential of 3.1 V/SHE, the 196.7 Da product was not observed, indicating it was further oxidized at this potential.

Figure 4b shows the proposed chlorinated phenolic ($C_8H_7O_4Cl$) product, with a mass of 202.6 Da, which is similar to the target mass of the 202.1 Da. Furthermore, the proposed $C_8H_7O_4Cl$ product is similar to the proposed DHC compound (188.2 Da) that was assigned to the 187.2 Da product (Scheme 1). The peak area for DHC decreased as a function of NaCl addition at 3.1 V/SHE (Figure 3b), suggesting that it or a similar compound could be a precursor for $C_8H_7O_4Cl$ formation.

The electrochemical pathways leading to the formation of the proposed chlorinated organic byproducts are complex, and the fact that only one chlorinated product was observed at each potential makes any proposed pathway speculative. However, the detection of a single compound at each potential suggests that these products were fairly recalcitrant at the given anodic potential and solution conditions. Therefore, DFT simulations were conducted to determine the potential-dependent $\Delta G^{\ddagger}$ values for the oxidation of the proposed chlorinated products via DET (eq 4). Figure 4c shows the potential-dependent $\Delta G^{\ddagger}$

https://dx.doi.org/10.1021/acs.est.0c03916
Environ. Sci. Technol. 2020, 54, 12673−12683

Scheme 1. Proposed Mechanism of Resorcinol Electrooxidation in NaCl-Free Solutions[a]

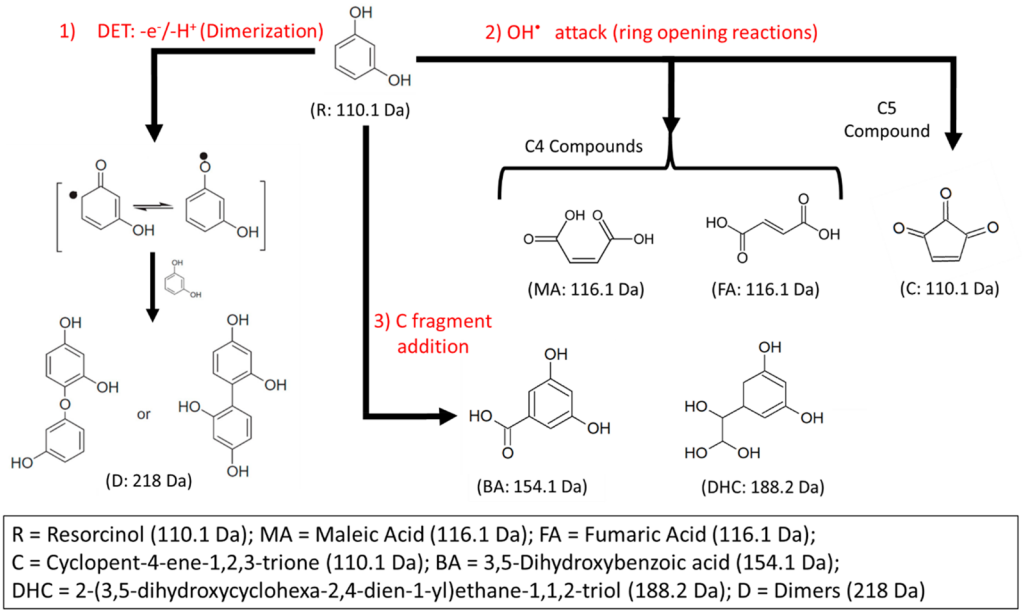

[a]Masses of compounds are for proposed structures and may differ slightly from masses detected by LC−MS (see Table S2).

values for the proposed chlorinated alcohol products ($C_3H_4OCl_4$ and $C_3H_2OCl_4$), and Figure 4d shows the potential-dependent $\Delta G^{\ddagger}$ values for the chlorinated phenolic product ($C_8H_7O_4Cl$). Modeling determined E° = 3.04 V/SHE and λ_f = 34 kJ mol^{-1} for $C_3H_2OCl_4$, E° = 4.06 V/SHE and λ_f = 97 kJ mol^{-1} for $C_3H_4OCl_4$, and E° = 1.94 V/SHE and λ_f = 25 kJ mol^{-1} for $C_8H_7O_4Cl$. Results suggest that both $C_3H_2OCl_4$ and $C_3H_4OCl_4$ were resistant to DET at 2.5 V/SHE, but oxidation of $C_3H_2OCl_4$ was feasible by DET at 3.1 V/SHE. For example, data in Figure 4c indicate that $\Delta G^{\ddagger}$ = 55 kJ mol^{-1} at 2.5 V/SHE and $\Delta G^{\ddagger}$ = 5.8 kJ mol^{-1} at 3.1 V/SHE for $C_3H_2OCl_4$ (195.9 Da) and $\Delta G^{\ddagger}$ = 93 kJ mol^{-1} at 3.1 V/SHE for $C_3H_4OCl_4$ (197.9 Da). Furthermore, additional DFT calculations indicated that the reactions between OH$^{\bullet}$ and $C_3H_2OCl_4$ were not thermodynamically favorable for either H-abstraction (reaction energy = 540 kJ mol^{-1}) or OH$^{\bullet}$ addition mechanisms (reaction energy = 435 to 449 kJ mol^{-1}). By contrast, DFT simulations estimated a reaction energy of −90 kJ mol^{-1} for the H-abstraction reaction between OH$^{\bullet}$ and $C_3H_4OCl_4$, indicating that this reaction is thermodynamically favorable. The SI contains product structures for the reactions discussed above (Figures S12−S15). These findings are consistent with experimental results that showed the 196.7 Da compound was detected at 2.5 V/SHE but was not detected at 3.1 V/SHE. That is, both $C_3H_2OCl_4$ and $C_3H_4OCl_4$ are expected to be oxidized at 3.1 V/SHE, the former via a DET mechanism and the latter via a OH$^{\bullet}$-mediated mechanism.

In addition, DFT simulations indicated that the $C_8H_7O_4Cl$ product would react by DET without an activation energy at both 2.5 V/SHE and at 3.1 V/SHE (Figure 4d). Similar to other phenolic compounds, the $C_8H_7O_4Cl$ compound is also expected to react readily with OH$^{\bullet}$, indicating it was likely a transient intermediate. Therefore, its detection at 3.1 V/SHE indicates that pathway 3, which leads to C fragment addition to resorcinol (Scheme 1), was likely a primary pathway for formation of chlorinated organic compounds.

Additional products from the oxidation of the two detected chlorinated products were not observed experimentally. The lack of detection of additional products was likely due to the formation of nonpolar C1 and C2 chlorinated products that were not detected by LC−MS or further reacted to form CO_2 and Cl^-.[72] Independent analyses were not conducted to quantify THMs or HAAs using standard methods. However, HAAs were expected to be detected with our LC−MS method, but the detection limit was not quantified. Therefore, further work is needed to characterize THMs, HAAs, and other nonpolar compounds and determine their concentrations relative to other EAOP electrodes.

Environmental Significance. The results reported in this study are the critical first step in understanding chlorinated byproduct formation on Ti_4O_7 electrodes under anodic conditions. Although it may be possible to eliminate all chlorinated organic byproducts through a combination of direct and indirect oxidation reactions, accomplishing this goal would require long residence times in the electrochemical cell, which in turn would favor ClO_4^- formation. The use of Ti_4O_7 REMs for potable water treatment applications will require optimization of operating conditions and possibly a multi-barrier approach. Coupling an appropriate cathode material downstream of the Ti_4O_7 anode may be necessary to dehalogenate the halogenated organics that form under anodic conditions. Recently a carbon-composite Ti_4O_7 cathode was shown to efficiently dehalogenate a range of halogenated acetic acid compounds to below regulatory standards.[73] These tandem strategies need to be tested experimentally to determine their feasibility compared to conventional approaches (e.g., activated carbon). Further work is also needed to understand the roles that different NOM functional groups have on halogenated byproduct formation.

■ ASSOCIATED CONTENT

Supporting Information

The Supporting Information is available free of charge at https://pubs.acs.org/doi/10.1021/acs.est.0c03916.

https://dx.doi.org/10.1021/acs.est.0c03916
Environ. Sci. Technol. 2020, 54, 12673−12683

Reactor setup schematic; possible byproduct formation pathway scheme; HPLC and chemical oxygen demand measurements; perchlorate formation results; LC−MS results; NaOCl/resorcinol product formation; masses of detected and proposed compounds; geometric optimized DFT structures (PDF)

AUTHOR INFORMATION

Corresponding Author

Brian P. Chaplin − *Department of Chemical Engineering, University of Illinois at Chicago, Chicago, Illinois 60607, United States;* orcid.org/0000-0003-1668-5414; Phone: +13129960288; Email: chaplin@uic.edu

Authors

Meng-Hsuan Lin − *Department of Chemical Engineering, University of Illinois at Chicago, Chicago, Illinois 60607, United States*

Devon Manley Bulman − *Environmental Chemistry and Technology Program, University of Wisconsin-Madison, Madison, Wisconsin 53706, United States*

Christina K. Remucal − *Environmental Chemistry and Technology Program and Department of Civil and Environmental Engineering, University of Wisconsin-Madison, Madison, Wisconsin 53706, United States;* orcid.org/0000-0003-4285-7638

Complete contact information is available at: https://pubs.acs.org/10.1021/acs.est.0c03916

Notes

The authors declare no competing financial interest.

ACKNOWLEDGMENTS

Funding for this work for BPC was provided by the National Science Foundation (CBET-1453081; CBET-1604776). Funding for CKR was provided by the National Science Foundation (CBET-1451932).

REFERENCES

(1) Mccarty, P. L.; Bae, J.; Kim, J. Domestic Wastewater Treatment as a Net Energy Producer-Can This Be Achieved? *Environ. Sci. Technol.* **2011**, *45*, 7100−7106.

(2) Comninellis, C. H.; Pulgarin, C. Anodic Oxidation of Phenol for Waste Water Treatment. *J. Appl. Electrochem.* **1991**, *21*, 703−708.

(3) Martínez-Huitle, C. A.; Ferro, S. Electrochemical Oxidation of Organic Pollutants for the Wastewater Treatment: Direct and Indirect Processes. *Chem. Soc. Rev.* **2006**, *35*, 1324−1340.

(4) Brillas, E.; Sirés, I. Electrochemical Removal of Pharmaceuticals from Water Streams: Reactivity Elucidation by Mass Spectrometry. *TrAC, Trends Anal. Chem.* **2015**, *70*, 112−121.

(5) Schaefer, C. E.; Choyke, S.; Ferguson, P. L.; Andaya, C.; Burant, A.; Maizel, A.; Strathmann, T. J.; Higgins, C. P. Electrochemical Transformations of Perfluoroalkyl Acid (PFAA) Precursors and PFAAs in Groundwater Impacted with Aqueous Film Forming Foams. *Environ. Sci. Technol.* **2018**, *52* (18), 10689−10697.

(6) Schaefer, C. E.; Andaya, C.; Urtiaga, A.; Mckenzie, E. R.; Higgins, C. P. Electrochemical Treatment of Perfluorooctanoic Acid (PFOA) and Perfluorooctane Sulfonic Acid (PFOS) in Groundwater Impacted by Aqueous Film Forming Foams (AFFFs). *J. Hazard. Mater.* **2015**, *295*, 170−175.

(7) Chaplin, B. P. Critical Review of Electrochemical Advanced Oxidation Processes for Water Treatment Applications. *Environ. Sci. Process. Impacts* **2014**, *16* (6), 1182−1203.

(8) Mayer, B. K.; Ryan, D. R. Impact on Disinfection Byproducts Using Advanced Oxidation Processes for Drinking Water Treatment. *Appl. of Advanced Oxid. Process. Drink. Water Treat.* **2017**, *67*, 345−386.

(9) Cornejo, O. M.; Murrieta, M. F.; Castañeda, L. F.; Nava, J. L. Characterization of the Reaction Environment in Flow Reactors Fitted with BDD Electrodes for Use in Electrochemical Advanced Oxidation Processes: A Critical Review. *Electrochim. Acta* **2020**, *331*, 1−14.

(10) Henke, A. H.; Saunders, T. P.; Pedersen, J. A.; Hamers, R. J. Enhancing Electrochemical Efficiency of Hydroxyl Radical Formation on Diamond Electrodes by Functionalization with Hydrophobic Monolayers. *Langmuir* **2019**, *35* (6), 2153−2163.

(11) Bagastyo, A. Y.; Batstone, D. J.; Kristiana, I.; Gernjak, W.; Joll, C.; Radjenovic, J. Electrochemical Oxidation of Reverse Osmosis Concentrate on Boron-Doped Diamond Anodes at Circumneutral and Acidic pH. *Water Res.* **2012**, *46* (18), 6104−6112.

(12) Anglada, Á.; Urtiaga, A.; Ortiz, I.; Mantzavinos, D.; Diamadopoulos, E. Boron-Doped Diamond Anodic Treatment of Landfill Leachate: Evaluation of Operating Variables and Formation of Oxidation By-Products. *Water Res.* **2011**, *45* (2), 828−838.

(13) Boudreau, J.; Bejan, D.; Bunce, N. J. Competition between Electrochemical Advanced Oxidation and Electrochemical Hypochlorination of Acetaminophen at Boron-Doped Diamond and Ruthenium Dioxide Based Anodes. *Can. J. Chem.* **2010**, *88* (5), 418−425.

(14) Bagastyo, A. Y.; Batstone, D. J.; Kristiana, I.; Escher, B. I.; Joll, C.; Radjenovic, J. Electrochemical Treatment of Reverse Osmosis Concentrate on Boron-Doped Electrodes in Undivided and Divided Cell Configurations. *J. Hazard. Mater.* **2014**, *279*, 111−116.

(15) Bagastyo, A. Y.; Batstone, D. J.; Rabaey, K.; Radjenovic, J. Electrochemical Oxidation of Electrodialysed Reverse Osmosis Concentrate on Ti/Pt-IrO_2, Ti/SnO_2-Sb and Boron-Doped Diamond Electrodes. *Water Res.* **2013**, *47* (1), 242−250.

(16) Bergmann, M. E. H.; Rollin, J.; Iourtchouk, T. The Occurrence of Perchlorate during Drinking Water Electrolysis Using BDD Anodes. *Electrochim. Acta* **2009**, *54* (7), 2102−2107.

(17) Azizi, O.; Hubler, D.; Schrader, G.; Farrell, J.; Chaplin, B. P. Mechanism of Perchlorate Formation on Boron-Doped Diamond Film Anodes. *Environ. Sci. Technol.* **2011**, *45*, 10582−10590.

(18) Hubler, D. K.; Baygents, J. C.; Chaplin, B. P.; Farrell, J. Understanding Chlorite and Chlorate Formation Associated with Hypochlorite Generation at Boron Doped Diamond Film Anodes. *J. Electrochem. Soc.* **2014**, *161* (12), E182−E189.

(19) Singer, P. C. Control of Disinfection By-Products in Drinking Water. *J. Environ. Eng.* **1994**, *120* (4), 727−744.

(20) Florentin, A.; Hautemanière, A.; Hartemann, P. Health Effects of Disinfection By-Products in Chlorinated Swimming Pools. *Int. J. Hyg. Environ. Health* **2011**, *214* (6), 461−469.

(21) Environmental Protection Agency (EPA). *National Primary Drinking Water Regulations: Proposed Perchlorate Rule*; U.S. EPA, 2018.

(22) Massachusetts, Dept. of Env. Protection. *Drinking Water Standard for Perchlorate*; Massachusetts Department of Environmental Protection, 2006.

(23) California, Dept. of Toxic Substances Control. *Perchlorate Maximum Contaminant Level (MCL) Review*; DTSC CA, 2015.

(24) Environmental Protection Agency (EPA). *Third Unregulated Contaminant Monitoring Rule (UCMR 3): Data Summary*; U.S. EPA, 2017.

(25) Sharma, V. K.; Yang, X.; Cizmas, L.; McDonald, T. J.; Luque, R.; Sayes, C. M.; Yuan, B.; Dionysiou, D. D. Impact of Metal Ions, Metal Oxides, and Nanoparticles on the Formation of Disinfection Byproducts during Chlorination. *Chem. Eng. J.* **2017**, *317*, 777−792.

(26) Hayfield, P. C. S. *Development of a New Material- Monolithic Ti_4O_7 Ebonex® Ceramic*; Royal Society of Chemistry, 2002.

(27) Jing, Y.; Almassi, S.; Mehraeen, S.; LeSuer, R. J.; Chaplin, B. P. The Roles of Oxygen Vacancies, Electrolyte Composition, Lattice Structure, and Doping Density on the Electrochemical Reactivity of Magnéli Phase TiO_2 Anodes. *J. Mater. Chem. A* **2018**, *6* (46), 23828−23839.

(28) Le, T. X. H.; Haflich, H.; Shah, A. D.; Chaplin, B. P. Energy-Efficient Electrochemical Oxidation of Perfluoroalkyl Substances Using a Ti_4O_7 Reactive Electrochemical Membrane Anode. *Environ. Sci. Technol. Lett.* **2019**, *6* (8), 504−510.
(29) Trellu, C.; Chaplin, B. P.; Coetsier, C.; Esmilaire, R.; Cerneaux, S.; Causserand, C.; Cretin, M. Electro-Oxidation of Organic Pollutants by Reactive Electrochemical Membranes. *Chemosphere* **2018**, *208*, 159−175.
(30) Zaky, A. M.; Chaplin, B. P. Porous Substoichiometric TiO_2 Anodes as Reactive Electrochemical Membranes for Water Treatment. *Environ. Sci. Technol.* **2013**, *47* (12), 6554−6563.
(31) Zaky, A. M.; Chaplin, B. P. Mechanism of p-Substituted Phenol Oxidation at a Ti_4O_7 Reactive Electrochemical Membrane. *Environ. Sci. Technol.* **2014**, *48* (10), 5857−5867.
(32) Guo, L.; Jing, Y.; Chaplin, B. P. Development and Characterization of Ultrafiltration TiO_2 Magnéli Phase Reactive Electrochemical Membranes. *Environ. Sci. Technol.* **2016**, *50* (3), 1428−1436.
(33) Gayen, P.; Chen, C.; Abiade, J. T.; Chaplin, B. P. Electrochemical Oxidation of Atrazine and Clothianidin on Bi-Doped SnO_2-Ti_nO_{2n-1} Electrocatalytic Reactive Electrochemical Membranes. *Environ. Sci. Technol.* **2018**, *52* (21), 12675−12684.
(34) Misal, S. N.; Lin, M. H.; Mehraeen, S.; Chaplin, B. P. Modeling Electrochemical Oxidation and Reduction of Sulfamethoxazole Using Electrocatalytic Reactive Electrochemical Membranes. *J. Hazard. Mater.* **2020**, *384*, 1−12.
(35) Canizares, P.; Martınez, F.; Dıaz, M.; Garcıa-Gomez, J.; Rodrigo, M. A. Electrochemical Oxidation of Aqueous Phenol Wastes Using Active and Nonactive Electrodes. *J. Electrochem. Soc.* **2002**, *149* (8), D118−D124.
(36) Nady, H.; El-Rabiei, M. M.; El-Hafez, G. M. A. Electrochemical Oxidation Behavior of Some Hazardous Phenolic Compounds in Acidic Solution. *Egypt. J. Pet.* **2017**, *26* (3), 669−678.
(37) Enache, T. A.; Oliveira-Brett, A. M. Phenol and Para-Substituted Phenols Electrochemical Oxidation Pathways. *J. Electroanal. Chem.* **2011**, *655* (1), 9−16.
(38) Nayak, S.; Chaplin, B. P. Fabrication and Characterization of Porous, Conductive, Monolithic Ti_4O_7 Electrodes. *Electrochim. Acta* **2018**, *263*, 299−310.
(39) Lee, S.; Lee, G.-H.; Kim, J.-C.; Kim, D.-W. Magneíi-Phase Ti_4O_7 Nanosphere Electrocatalyst Support for Carbon-Free Oxygen Electrodes in Lithium-Oxygen Batteries. *ACS Catal.* **2018**, *8*, 2601−2610.
(40) Wang, G.; Liu, Y.; Ye, J.; Qiu, W.; Ma, S.; An, X. Fabrication of Rod-like Ti_4O_7 with High Conductivity by Molten Salt Synthesis. *Mater. Lett.* **2017**, *186*, 361−363.
(41) Almassi, S.; Li, Z.; Xu, W.; Pu, C.; Zeng, T.; Chaplin, B. P. Simultaneous Adsorption and Electrochemical Reduction of N-Nitrosodimethylamine Using Carbon-Ti_4O_7 Composite Reactive Electrochemical Membranes. *Environ. Sci. Technol.* **2019**, *53* (2), 928−937.
(42) Snoeyink, V. L., Jenkins, D. *Water Chemistry*; John Wiley and Sons: New York, 1980.
(43) Gayen, P.; Chaplin, B. P. Fluorination of Boron-Doped Diamond Film Electrodes for Minimization of Perchlorate Formation. *ACS Appl. Mater. Interfaces* **2017**, *9*, 27638−27648.
(44) Mikolajczyk, T.; Pierozynski, B.; Smoczynski, L.; Wiczkowski, W. Electrodegradation of Resorcinol on Pure and Catalyst-Modified Ni Foam Anodes, Studied under Alkaline and Neutral pH Conditions. *Molecules* **2018**, *23* (6), 1293−1304.
(45) Yates, R. L.; Havery, D. C. Determination of Phenol, Resorcinol, Salicylic Acid and α-Hydroxy Acids in Cosmetic Products and Salon Preparations. *J. Cosmet. Sci.* **1999**, *50* (5), 315−325.
(46) HACH. *Chemical Oxygen Demand, Dichromate Method*; HACH, **2014**; Vol. *DOC316.53*.
(47) Frisch, M. J. T. G. W.; Schlegel, H. B.; Scuseria, G. E.; Robb, M. A.; Cheeseman, J. R.; Scalmani, G.; Barone, V.; Petersson, G. A.; Nakatsuji, H.; Li, X.; Caricato, M.; Marenich, A. V.; Bloino, J.; Janesko, B. G.; Gomperts, R.; Mennucci, B.; Hratchian, H. P.; Ortiz, J. V.; Izmaylov, A. F.; Sonnenberg, J. L.; Williams-Young, D.; Ding, F.; Lipparini, F.; Egidi, F.; Goings, J.; Peng, B.; Petrone, A.; Henderson, T.; Ranasinghe, D.; Zakrzewski, V. G.; Gao, J.; Rega, N.; Zheng, G.; Liang, W.; Hada, M.; Ehara, M.; Toyota, K.; Fukuda, R.; Hasegawa, J.; Ishida, M.; Nakajima, T.; Honda, Y.; Kitao, O.; Nakai, H.; Vreven, T.; Throssell, K.; Montgomery, J. A., Jr.; Peralta, J. E.; Ogliaro, F.; Bearpark, M. J.; Heyd, J. J.; Brothers, E. N.; Kudin, K. N.; Staroverov, V. N.; Keith, T. A.; Kobayashi, R.; Normand, J.; Raghavachari, K.; Rendell, A. P.; Burant, J. C.; Iyengar, S. S.; Tomasi, J.; Cossi, M.; Millam, J. M.; Klene, M.; Adamo, C.; Cammi, R.; Ochterski, J. W.; Martin, R. L.; Morokuma, K.; Farkas, O.; Foresman, J. B.; Fox, D. J. *Gaussian 16*, Revision B.01; Gaussian, Inc.: Wallingford CT, 2016.
(48) Zhao, Y.; Truhlar, D. G. The M06 Suite of Density Functionals for Main Group Thermochemistry, Thermochemical Kinetics, Noncovalent Interactions, Excited States, and Transition Elements: Two New Functionals and Systematic Testing of Four M06-Class Functionals and 12 Other Functionals. *Theor. Chem. Acc.* **2008**, *120* (1−3), 215−241.
(49) Marenich, A. V.; Cramer, C. J.; Truhlar, D. G. Universal Solvation Model Based on Solute Electron Density and on a Continuum Model of the Solvent Defined by the Bulk Dielectric Constant and Atomic Surface Tensions. *J. Phys. Chem. B* **2009**, *113* (18), 6378−6396.
(50) Jing, Y.; Chaplin, B. P. Mechanistic Study of the Validity of Using Hydroxyl Radical Probes to Characterize Electrochemical Advanced Oxidation Processes. *Environ. Sci. Technol.* **2017**, *51* (4), 2355−2365.
(51) Kelly, C. P.; Cramer, C. J.; Truhlar, D. G. Aqueous Solvation Free Energies of Ions and Ion-Water Clusters Based on an Accurate Value for the Absolute Aqueous Solvation Free Energy of the Proton. *J. Phys. Chem. B* **2006**, *110* (32), 16066−16081.
(52) Tissandier, M. D.; Cowen, K. A.; Feng, W. Y.; Gundlach, E.; Cohen, M. H.; Earhart, A. D.; Coe, J. V.; Tuttle, T. R. The Proton's Absolute Aqueous Enthalpy and Gibbs Free Energy of Solvation from Cluster-Ion Solvation Data. *J. Phys. Chem. A* **1998**, *102* (40), 7787−7794.
(53) Bard, A. J.; Faulkner, L. R. *Electrochemical Methods: Fundamentals and Applications*, 2nd ed.; Wiley Second. John Wiley and Sons, 2001.
(54) Vaissier, V.; Barnes, P.; Kirkpatrick, J.; Nelson, J. Influence of Polar Medium on the Reorganization Energy of Charge Transfer between Dyes in a Dye Sensitized Film. *Phys. Chem. Chem. Phys.* **2013**, *15* (13), 4804−4814.
(55) Donaghue, A.; Chaplin, B. P. Effect of Select Organic Compounds on Perchlorate Formation at Boron-Doped Diamond Film Anodes. *Environ. Sci. Technol.* **2013**, *47* (21), 12391−12399.
(56) Arnold, W. A.; Bolotin, J.; Gunten, U.; Hofstetter, T. B. Evaluation of Functional Groups Responsible for Chloroform Formation during Water Chlorination Using Compound Specific Isotope Analysis. *Environ. Sci. Technol.* **2008**, *42* (21), 7778−7785.
(57) Tretyakova, N. Y.; Lebedev, A. T.; Petrosyan, V. S. Degradative Pathways for Aqueous Chlorination of Orcinol. *Environ. Sci. Technol.* **1994**, *28* (4), 606−613.
(58) Lin, S.; Liukkonen, R. J.; Thom, R. E.; Bastian, J. G.; Lukasewycz, M. T.; Carlson, R. M. Increased Chloroform Production from Model Components of Aquatic Humus and Mixtures of Chlorine Dioxide/Chlorine. *Environ. Sci. Technol.* **1984**, *18* (12), 932−935.
(59) Jackson, D. E.; Larson, R. A.; Snoeyink, V. L. Reactions of Chlorine and Chlorine Dioxide with Resorcinol in Aqueous Solution and Adsorbed on Granular Activated Carbon. *Water Res.* **1987**, *21* (7), 849−857.
(60) Gan, W.; Ge, Y.; Zhu, H.; Huang, H.; Yang, X. ClO_2 Pre-Oxidation Changes the Yields and Formation Pathways of Chloroform and Chloral Hydrate from Phenolic Precursors during Chlorination. *Water Res.* **2019**, *148*, 250−260.
(61) Ge, F.; Zhu, L.; Chen, H. Effects of pH on the Chlorination Process of Phenols in Drinking Water. *J. Hazard. Mater.* **2006**, *133* (1−3), 99−105.

https://dx.doi.org/10.1021/acs.est.0c03916
Environ. Sci. Technol. 2020, 54, 12673−12683

(62) Tak, S.; Prakash Vellanki, B. Natural Organic Matter as Precursor to Disinfection Byproducts and Its Removal Using Conventional and Advanced Processes: State of the Art Review. *J. Water Health* **2018**, *16* (5), 681−703.
(63) Hussein, A. A.; Al-Hadedi, A. A. M.; Mahrath, A. J.; Moustafa, G. A. I.; Almalki, F. A.; Alqahtani, A.; Shityakov, S.; Algazally, M. E. Mechanistic Investigations on Pinnick Oxidation: A Density Functional Theory Study. *R. Soc. Open Sci.* **2020**, *7* (2), 191568.
(64) Nihemaiti, M.; Le Roux, J.; Hoppe-Jones, C.; Reckhow, D. A.; Croué, J.-P. Formation of Haloacetonitriles, Haloacetamides, and Nitrogenous Heterocyclic Byproducts by Chloramination of Phenolic Compounds. *Environ. Sci. Technol.* **2017**, *51* (1), 655−663.
(65) Boyce, S. D.; Hornig, J. F. Reaction Pathways of Trihalomethane Formation from the Halogenation of Dihydroxyaromatic Model Compounds for Humic Acid. *Environ. Sci. Technol.* **1983**, *17* (37), 297−309.
(66) Rook, J. J. Chlorination Reactions of Fulvic Acids in Natural Waters. *Environ. Sci. Technol.* **1977**, *11* (5), 478−482.
(67) Kapałka, A.; Fóti, G.; Comninellis, C. The Importance of Electrode Material in Environmental Electrochemistry: Formation and Reactivity of Free Hydroxyl Radicals on Boron-Doped Diamond Electrodes. *Electrochim. Acta* **2009**, *54* (7), 2018−2023.
(68) Buxton, G. V.; Greenstock, C. L.; Helman, W. P.; Ross, A. B. Critical Review of Rate Constants for Reactions of Hydrated Electrons, Hydrogen Atoms and Hydroxyl Radicals (·OH/·O^- in Aqueous Solution. *J. Phys. Chem. Ref. Data* **1988**, *17* (2), 513−886.
(69) Enache, T. A.; Oliveira-Brett, A. M. Phenol and Para-Substituted Phenols Electrochemical Oxidation Pathways. *J. Electroanal. Chem.* **2011**, *655* (1), 9−16.
(70) Bensalah, N.; Abdellatif, G.; Cañizares, P.; Sáez, C.; Lobato, J.; Rodrigo, M. A. Electrochemical Oxidation of Hydroquinone, Resorcinol, and Catechol on Boron-Doped Diamond Anodes. *Environ. Sci. Technol.* **2005**, *39* (18), 7234−7239.
(71) Arnold, W. A.; Bolotin, J.; Von Gunten, U.; Hofstetter, T. B. Evaluation of Functional Groups Responsible for Chloroform Formation during Water Chlorination Using Compound Specific Isotope Analysis. *Environ. Sci. Technol.* **2008**, *42* (21), 7778−7785.
(72) Mousset, E.; Oturan, N.; Oturan, M. A. An Unprecedented Route of ·OH Radical Reactivity Evidenced by an Electrocatalytical Process: Ipso-Substitution with Perhalogenocarbon Compounds. *Appl. Catal., B* **2018**, *226*, 135−146.
(73) Almassi, S.; Samonte, P. R. V.; Li, Z.; Xu, W.; Chaplin, B. P. Mechanistic Investigation of Haloacetic Acid Reduction Using Carbon-Ti_4O_7 Composite Reactive Electrochemical Membranes. *Environ. Sci. Technol.* **2020**, *54* (3), 1982−1991.

https://dx.doi.org/10.1021/acs.est.0c03916
Environ. Sci. Technol. 2020, 54, 12673−12683